Discovery and characterization of submarine groundwater discharge in the Siberian Arctic seas: A case study in Buor-Khaya Gulf, Laptev Sea

Alexander N. Charkin[1,2], Michiel Rutgers van der Loeff[3], Natalia E. Shakhova[2,4], Örjan Gustafsson[5], Oleg V. Dudarev[1,2], Maxim S. Cherepnev[2], Anatoly N. Salyuk[1], Andrey V. Koshurnikov[6], Eduard A. Spivak[1], Alexey Y. Gunar[6], Igor P. Semiletov[1,2,4]

[1]Pacific Oceanological Institute (POI), Far Eastern Branch of Russian Academy of Sciences Russian Academy of Sciences (FEBRAS) , Vladivostok, Russia
[2]National Research Tomsk Polytechnic University, Russia
[3]Alfred-Wegener Institute, Helmholtz Center for Polar and Marine Research, Bremerhaven, Germany
[4]International Arctic Research Center (IARC), University of Alaska, Fairbanks, USA
[5]Dept. of Environmental Science and Analytical Chemistry, and the Bolin Centre for Climate Research, Stockholm University, Stockholm, Sweden
[6]Moscow State University, Russia

Correspondence to: Alexander N. Charkin (charkin@poi.dvo.ru)

Abstract. It has been suggested that increasing freshwater discharge to the Arctic Ocean may also occur as submarine groundwater discharge (SGD), yet there are no direct observations of this phenomenon in the Arctic shelf seas. This study tests the hypothesis that SGD does exist in the Siberian-Arctic shelf seas but its dynamics may be largely controlled by complicated geocryological conditions such as permafrost. The field-observational approach in the southeast Laptev Sea used a combination of hydrological (temperature, salinity), geological (bottom sediment drilling, geoelectric surveys) and geochemical (^{224}Ra, ^{223}Ra and ^{222}Rn) techniques. Active SGD was documented in the vicinity of the Lena River delta with two different operational modes. In the first system, groundwater discharges through tectonogenic permafrost talik zones was registered in both wintertime and summertime seasons. The second SGD mechanism was cryogenic squeezing out of brine and water-soluble salts detected on the periphery of ice hummocks in the wintertime season. The proposed mechanisms of groundwater transport and discharge in the arctic land-shelf system is elaborated. Through salinity versus ^{224}Ra and ^{224}Ra/^{223}Ra diagrams, the three main SGD-influenced water masses were identified and their end-member composition was constrained. Further studies should apply these techniques to a broader scale with the objective to reach an estimate of the relative importance of the SGD transport vector relative to surface freshwater discharge for both the water balance and aquatic components such as dissolved organic carbon, carbon dioxide, methane, and nutrients.

1 Introduction

The Arctic system constitutes a unique and important environment with a central role in the dynamics and evolution of the earth system. Global warming has regional effects on the Arctic, including on all cryospheric features. Energy and water fluxes shape the regional temperature regime, which is a primary factor in determining the physical state (frozen vs. thawed), trace gas fluxes, rates of productivity, and the link to regional climate (Serreze et al., 2006; Vörösmarty et al. 2000; Shakhova et al., 2010, 2014; Semiletov et al., 2007, 2016; Vonk et al., 2012).

The Arctic is inherently a highly dynamic system. Yet there is mounting evidence that it is now experiencing an unprecedented degree of environmental change. Many of these changes are linked to the Arctic hydrologic cycle. The delivery of freshwater (FW) from the continental land mass is of special importance to the Arctic Ocean since it contains only 1% of the World 's ocean water, yet receives 11% of World river runoff (Shiklomanov et al. 2000). The

5 Arctic Ocean is the most river-influenced and landlocked of all oceans and is the only ocean surrounded by permafrost with a drainage basin area greater than its surface area (Semiletov et al., 2000, 2012; Vörösmarty et al., 2000; Macdonald et al., 2008). Annual FW inflow contributes as much as 10% of the freshwater in the upper 100 meters of the water column for the entire Arctic Ocean (Barry and Serreze 2000). Approximately three-quarters of Arctic Ocean riverine freshwater input derives from the Eurasian portion of the Arctic Ocean watershed, and three rivers (Yenisei,

10 Lena, Ob) are responsible for approximately 70% of this contribution (Carmack 1990; Gordeev et al. 1996). This water exerts a tremendous influence on the Arctic Ocean and especially on the Eurasian shelf seas (the Barents, Kara, Laptev, and East Siberian Seas). Salinity distribution and sea ice formation are affected by continental runoff. The cumulative impact of changes in FW flux to the Arctic Ocean may exert significant control over global ocean circulation by affecting the volume of North Atlantic Deep Water formation (IPCC, 2013).

15 Since the first reports of increases in winter and total discharge for several Great Eurasian Arctic rivers (Savelieva et al., 2000; Semiletov et al., 2000), many studies have reported remarkable changes in water cycle components of the northern hydrological systems, such as increases of Yenisei, Lena, Ob river runoff and changes in their seasonal pattern of discharge (Peterson et al., 2002; McClelland et al., 2006; Serreze et al., 2006). Arctic and subarctic watersheds are undergoing climate warming, permafrost thawing, and thermokarst formation resulting in quantitative

20 shifts in surface water –groundwater interaction at the basin scale. The Lena River region is a prioritized study object as changes in the Lena River hydrology play a significant role in feeding the Transarctic Drift through change in the FW export to the Laptev Sea. The Lena River is also a natural boundary between Western and Eastern Siberia: in atmospheric circulation patterns – land hydrology – sea ice condition, tectonic structure, and biological peculiarities on the Siberian shelf (Semiletov et al., 2000). Most of the Lena river basin is underlain by permafrost: about 79% with

25 continuous permafrost, and the remainder with discontinuous permafrost (Zhang et al., 2005), while large West Siberian rivers (Ob and Yenisei) are situated mainly in non-permafrost and/or discontinuous permafrost.

A hypothetical contribution/mechanism of submarine groundwater discharge (SGD) is schematically shown in Fig. 1. SGD is a mixture of fresh groundwater and seawater that has recirculated through the subterranean estuary as result of tides and wave action, which discharges to the ocean (Moore, 1999). It is estimated that groundwater currently

30 comprises almost one fourth of Yukon River water discharged to the Bering Sea, which subsequently is transported into the Arctic Ocean via Bering Strait (Walvoord and Striegl, 2000). Long-term streamflow records (>30 yrs) of the Yukon River basin indicate a general upward trend in groundwater contribution to streamflow of 0.7–0.9%/yr. Changes in the base flow, such as the increases in the Yenisei River between 1936 and 1995 (Vörösmarty et al., 2000), are also thought to reflect increased groundwater infiltration, coupled to reductions in permafrost and an increase in

35 active layer thickness due to warmer temperatures. Recent studies using Gravity Recovery and Climate Experiment (GRACE) have revealed a significant increase in subsurface terrestrial water storage in the Lena basin (Velicogna et al., 2012), which will have a significant impact on the terrestrial hydrology of the region, including increased base flow and alteration of seasonal runoff.

As of today, the Arctic Ocean shelf groundwater systems as well as the particularities of the SGD have been very

40 poorly studied. At the same time, groundwater systems of deep-seated subsurface aquifer systems have developed under the seafloor, which are similar to those on land (Hathaway et al., 1979, Kohout et., al., 1988, Bisson, 1994, Moore, 1999). In these systems, the migration of infiltration water is possible from the land, and the reverse, the

migration of saline water from the submarine watershed to the land. The origin and functioning of local SGD zones on the shelf is tightly connected via structural, lithological and geomorphological features to the shelf regions. For the Arctic shelf, with boundaries of widely developed permafrost, these subsurface land-sea interactions are complicated by the geocryological conditions. The permafrost is cementing rocks and forming a cryogenically-confining bed

5   (impermeable frozen rocks) (Pinneker, 1983; Romanovskii, 1983).

Until recently, knowledge about the present thermal state of subsea permafrost was mainly based on controversial modeling results. Some authors suggest that it would take ~5-7 millennia for subsea permafrost to reach the thaw point (Romanovskii et al., 2005), meaning that the coastal subsea permafrost is still stable. Others believe that in the coastal areas of the shallow Siberian Arctic seas, where permafrost was submerged most recently, *taliks* (layers or columns

10 of thawed sediments within permafrost) might form as the result of the combined effect of geothermal flux from fault zones, the warming effect of rivers and overlying seawater, and the already present thermokarst (Shakhova and Semiletov, 2007; Shakhova et al., 2009, 2015; Nicolsky and Shakhova, 2010; Nicolsky et al., 2012). Moreover, the first results from off-shore drilling (accomplished from the fast ice in April 2011) down to 52 m below the sea floor in the southeastern Laptev Sea, showed that the sediment core was entirely unfrozen, and 8-12 C warmer than on-land

15 sediment core obtained in the nearby Chay-Tumus borehole (Shakhova et al., 2014) – confirming these author's modeling results.

This study employs state-of-the-art measurements of the radium isotope quartette (^{224}Ra, half life = 3.66 days; ^{223}Ra, half life = 11.4 days; ^{228}Ra, half life = 5.75 years; ^{226}Ra, half life = 1600 years) and radon (^{222}Rn, half life = 3.82 days). These naturally-occurring isotopes are useful tracers in the environment for measuring coastal ocean mixing rates

20 (Moore, 1996, 2000a; Charrette et al., 2003, 2007, 2013; Hancock et al., 2006, Gonneea et al., 2008), ages of river plumes (Moore and Krest, 2004; Gu et al., 2012), estuarine residence times (Moore et al., 2006; Rapaglia et al., 2010), and as indicators of SGD (Rama and Moore, 1996; Charrette et al., 2008). One must note that this research was to date conducted in the seas and estuaries of moderate, subtropical and tropical climates, and with rare exceptions, in the Arctic seas. Work in the Arctic seas have so far largely relied on long-lived isotopes ^{228}Ra and ^{226}Ra (Rutgers van

25 der Loeff et al., 1995, 2003, 2012; Kadko, et al., 2008, 2009), with a very limited number of studies conducted only during the summer season, using short-lived isotopes ^{223}Ra, ^{224}Ra and ^{222}Rn, conducted only in the seas of the American side of the Arctic (Kadko, et al., 2008, 2009; Dimova et al., 2015; Lecher et al., 2015).

The main objective of this paper is to search for SGD in the Siberian Arctic area, assumed to be occupied by continuous subsea permafrost (Romanovskii et al., 1983). SGD is characterized using a combination of hydrological (temperature,

30 salinity), geological (bottom sediment drilling, geoelectric surveys) and geochemical (^{224}Ra, ^{223}Ra and ^{222}Rn) parameters. We focus our detailed analysis on the near-shore zone of the Laptev Sea – the northern extension of the Lena river basin, Eurasia, and a southern end of the Lena Rift (characterised by active seismo-tectonics, Imaev et. al., 2004), an area of about 2,400,000 km^2 in size. Finally, a mechanism of the SGD in this Arctic land-shelf system is proposed.

35

2 Material and methods

2.1 Field work

40 In situ observations, drilling and sampling were performed in the western part of the Buor-Khaya Bay of the Laptev Sea in the framework of the International Siberian Shelf Studies (ISSS, Semiletov and Gustafsson, 2009), and its extension, including subsea sediment drilling annually for five years (March-April of 2011-2015) (Fig. 2). Complex

exploratory survey were performed annually in March – April 2011 – 2015 on the southeastern Laptev Sea land-fast sea ice to drill bottom sediment (Shakhova et al., 2014). The central campaign equipment included a brand new drilling rig URB - 4T, transport caravan consisting of two caterpillars, a heavy all-terrain truck and a sled train (two two-storys mobile houses), hosting laboratory and accommodations. Drilling was accompanied by geoelectric survey

5   (Koshurnikov et al., 2016). Hydrological studies were also accomplished each year (2011-2015), including Conductivity-Temperature-Depth (CTD) (SeaBird 19Plus). The most detailed sampling for radium and radon activities was performed in March-April 2015. The choice of sampling sites was based on knowledge gained from drilling, oceanographic, and geoelectric data obtained in the four previous years.

Additional water samples were collected in September 2013 during the hydrological survey expedition "Lena Delta

10   2013" on board RV Dalnie Zelentsy (Gonçalves-Araujo et al., 2015).

2.2 Drilling and at-site characterization of bottom sediments

The subsea sediment boreholes were drilled from the land-fast ice in the spring using a rotary drill rig (URB-4T) and

15   a dry drilling technique. A metal casing was drilled through the fast ice, water column and into the sediment to prevent water from entering the borehole. Full methodology details can be found in (Shakhova et al., 2014). At-site laboratory investigation was performed immediately upon recovery and included sediment temperature and lithology.

2.3 Geoelectric surveys

20

Transient electrical method (TEM), aimed at the mapping of subsea permafrost table, determining the lithological structure and the search for taliks, was performed for each field campaign. A TCIKL-7 measuring device was used for the TEM fieldwork, as described in detail in Koshurnikov et al. (2016).

The TEM results in the area highlighted several layers with various resistivities. The boundary of these layers was

25   validated and confirmed first time by the subsea sediment drilling. The main conduction mechanism in earth materials is electrolytic, involving ion transport by dissolved salts distributed through a complex structure of interconnected pores and fractures. Resistivity of igneous and metamorphic rocks is typically high, while sedimentary rocks are usually much more conductive. Their resistivity is mainly controlled by the amount of water present, the salinity (free ions) of the water, and the degree of interconnections between the pores. Clay content can also contribute by providing

30   an additional surface conductivity mechanism (e.g., variations in grain size and pore space geometry) (Anderson et al., 1994). Resistivity of permafrost is typically high, low resistivity indicates that the layer is in the thawed state (Palacky, 1988). Further details on the employed methodology can be found elsewhere (Koshurnikov et al., 2016).

2.4 Hydrological surveys

35

The standard observations at each station started with a CTD measurement. A Seabird 19Plus CTD was used for measuring the vertical distribution of temperature and salinity. The device was used in a sounding mode. During winter campaign (2011-2015) an ice-hole was made at each station using a Jiffymotor drill. The sounding equipment was lowered by hand on a cable at a speed of around 1 m/s. For details of the summertime hydrological work during

40   Lena Delta 2013 see Gonçalves-Araujo et al., 2015.

2.5 Analytical methods

2.5.1 Sampling and measurements of ^{224}Ra and ^{223}Ra isotopes

5 In order to detect the possible outputs of SGD we collected water samples to measure the short-lived radium isotopes activity. Water samples (20-60 L) were pumped through the boreholes of the fast ice from surface (under the ice) and bottom (one meter from the bottom to avoid resuspension) water using Grundfos submersible pumps. At several stations the intermediate horizons were also sampled. At the shallow stations (6 m or less), the water samples were taken only from the middle horizon. Groundwater samples (5-20 L) were collected using the same submersible pumps

10 from the drilled bottom sediment borehole. The impermeability of the metal casing prevented seawater penetration into the borehole.

In the laboratory of the base camp, the water was subsequently pumped at < 1 L/min through a column of manganese-coated acrylic fiber (Mn fiber) to quantitatively capture dissolved radium (Moore, 1976; Moore and Arnold, 1996). After rinsing the Mn fiber samples with Ra-free deionized water to remove sea salts, they were partially dried and

15 placed in a closed-loop air circulation system as described in Moore and Arnold (1996). The Radium Delayed Coincidence Counter (RaDeCC) system utilizes the difference between the decay constants of the short-lived Po daughters of ^{219}Rn and ^{220}Rn to identify alpha particles derived from ^{219}Rn or ^{220}Rn decay and hence to determine activities of ^{223}Ra and ^{224}Ra on the Mn-fiber (Moore and Arnold, 1996). After the first ^{223}Ra and ^{224}Ra measurement in the laboratory of the base camp, Mn-fiber with radium samples were aged for 2-6 weeks to allow initial excess

20 ^{224}Ra to reach secular equilibrium with the ^{228}Th that had also absorbed on the Mn fiber. The samples were then measured again to determine ^{228}Th and thus to correct for supported ^{224}Ra (Moore and Arnold, 1996; Moore and Oliveira, 2008; Burnett et. al., 2008). The average statistical counting error was ± 8.5 % (range =± 5.6 - 39 %) for ^{223}Ra and ± 1.9 % (range = ± 1.4 - 19 %) for ^{224}Ra. We calibrated the RaDeCC systems for ^{224}Ra and ^{223}Ra measurements using ^{232}Th standards as described by Moore and Cai (2013).

25 Water samples collected during the Lena Delta 2013 expedition were immediately passed over Mn-coated acrylic fiber and analysed on board for the short-lived radium isotopes with RaDeCC following the same methods as described above. The analysis of supported activities in these samples was performed later in the home laboratory of AWI in Bremerhaven.

30 ### 2.5.2 Sampling and measurements of ^{222}Rn

Similar to short-lived radium isotopes, the ^{222}Rn can also be used for tracing SGD and has been measured in our studies. For the measurement of the volumetric radon activity in water samples we used the radiometer RRA-01M-03 produced by LLC "NTM-protection", Moscow, Russia, applying standard methods described in (Maintenance manual

35 Radiometer.., 2004). Radiometer RRA-01M-03 allows to measure the volumetric content of radon in the air and water, and was here adapted to regimes of Polar research (Stepanov and Egorova, 2004).

3 Results and Discussion

40 ### 3.1 Geologic, tectonic, and geoelectric settings in context of SGD characterization

The research area was located in the eastern part of the Laptev Sea, intensively studied all-seasonally by the author's team since 1994 (Semiletov, 1996; Semiletov et. al., 1999, 2013; Charkin et. al., 2011, 2015; Shakhova et al., 2014). Thus, a choice of the study area was based on a large original data sets obtained during >20 years, and literature data. According to the tectonic character, the study area is located in the northern part of Verkhoyansk Fold (Kharaulakh

5 Ridge), which apparently continues offshore and forms a pre-rift basement of the Ust Lena Rift (Fig. 3). The events of the Cenozoic history of this territory are related because the North American and the Eurasian plates are separated in the Eurasian Basin by the active mid-oceanic Gakkel Ridge, resulting in partial destruction of the continental crust over vast areas (Vinogradov and Drachev 2000; Franke et. al., 2001; Drachev, 2002; Imaev et. al., 2004). As the result of stretching during the Pliocene-Quaternary times, the graben borders formed young listric faults displacing the

10 weathering crust of the Neogene age, which are also well-known along the coast of the Buor-Khaya Gulf (Figs. 3, 4a). The stretching axis was oriented towards the northeast. These listric faults are observed in coastal outcrops from the Bykovsky distributaries in the delta of the Lena River to the Kharaulakh depression at a distance of more than 160 km (Fig. 4a) (Imaev et. al., 2004).

Seismic analysis on the shelf of the Laptev Sea shows that one of the most intense earthquake epicenters is located

15 precisely in our study area, and it coincides to the listric faults of the Ust-Lena graben borders 20 kilometers to the East from Bykovsky peninsula (Figs. 2, 3, 4a, c), according to data collected in the 1960-1990 period (Imaev, et. al., 2004). The listric fault displacement dominated focal mechanisms of earthquakes (Fig. 4c).

According to our TEM data, sharp resistivity contrasts were established in the area of the geophysical stations 2 and 3. The resistivity at the depth of more than 150 m falls from the West to the East from more than 350 to 80 Ω m,

20 locating the listric faults (Figs. 3, 4). These TEM results agree well with the data of Imaev et al for this region (Fig. 4) (Imaev, et. al., 2004). In TEM station No. 2; the resistivity did not exceed 1 - 9 Ω m up to the surface of the high resistance layer set at 162, 5 meters. This indicates the existence of open tectonogenic taliks here (Pinneker, 1983, Romanovskii, 1983), which coincide with the fault (Figs. 3, 4).

At the geoelectric sections, four deposition layers were distinguished, which differ by their lithology and temperature.

25 In all sections, which all had various thicknesses, low-resistance layers were discovered (1.7-3.4 Ω m), which testify to the presence of unfrozen rock (Koshurnikov et al., 2016). The drilling of wells 1D-15 established that this layer consisted of water-bearing sands (Fig. 4). In TEM station No. 2, in the surface depositions, we also discovered sedimentary strata with higher resistivity 8.3 Ω m and a thickness of 52 m, which was not discovered in the other sections. This stratum is probably the remainder of the Quaternary Ice Complex, which consists of loess deposits. As

30 the result of the sea transgression, this raised area was flooded, and it was possibly in part destroyed by thermal abrasion after sea transgression. As a result, due to the melting of relict ice and covering by recent sedimentary material, this area of the bottom was made level and is not clearly reflected in the recent relief (Figs. 2, 3, 4). A similar relict of the subaerial relief is the Muostakh Island, which is located on the surface of the footwall block of the neighboring listric faults (which, together with the listric faults being examined, form a listric fan). This island is

35 currently being intensively destroyed by thermal abrasion. If this assumption is true, then one can presume that the lithological composition of the shallow elements around Muostakh Island will have a similar composition with the sedimentary strata in TEM column No. 2 with a resistivity of 8,3 Ω m. According to our drilling results (4D-12), the lithological composition of the sediments is mainly represented by silty and clayed sediments (Fig. 4).

At three TEM stations, but not for station 2, a sharp change in resistivity can be noted from 1.7-2 Ω m water-bearing

40 sands to 35-80 Ω m, which is characteristic for permafrost (Fig. 4) (Koshurnikov et al., 2016; Palacky, G.J., 1988). Thus, it was determined by TEM that the depth of the subsea permafrost table in the study area (except for the talik

site) varies in the range from 20 to 46 meters. We also confirmed the correspondence of the subsea permafrost to this range of resistivity many times during the in-phase drilling and geoelectric surveys over many years (2011-2015).

3.2 Features of the thermohaline water structure vs SGD fate

5

The field campaigns in the northwestern part of the Buor-Khaya Gulf in 2015 were conducted during the winter low-discharge season. Due to its low winter flow, the influence of the Lena River under ice conditions is very restricted (Charkin et. al., 2011). Furthermore, there is no wind mixing, which together results in moderately and highly stratified water predominating in this region for this period (Figs. 5, 6, 7). Stratification factors, shown in Fig. 5, were

10 calculated according to (Burt et. al., 2014): whereby the mixed layer depth is divided by the water column depth; a stratification factor of one indicates a fully mixed water column. The salinity right under the ice near the delta ranged 0.04 - 3.1, while near the bottom it was 11.9-19.1, whereas at a distance from the delta these values varied from 5.8 to 13.9 under the ice and from 17.4 to 26.1 near the bottom (Figs. 6, 7).

In the area of stations 1516-1529, a plume of more saline water was discovered near the surface in comparison with

15 the surrounding waters (Fig. 6). Another larger lens of more saline water which was larger in size - around 7 km in width and more than 20 km in length, was discovered at a depth of 5-6 m (Fig. 6). Additionally, at stations 1529 and 1520, a local freshening of 0.5-1 in comparison with the neighboring stations was discovered near the bottom (Figs. 6, 7).

The temperature regime was characterized by ubiquitously negative values in the waters near the Delta (at stations

20 1502 and 1503). Under the influence of the river flow the surface water temperature was near 0°C (Figs. 6, 7). As in the case with the salinity anomalies described above, low-temperature anomalies were also discovered, which were structurally consistent with the lenses described above. In the vertical temperature profiles, this anomaly has a clear structure of a fluid with mushroom-like forms (Fig. 7) with an intrusion of low-temperature waters at the seafloor in the area of stations No. 1529 shaped by isohaline = 22.5. The temperature in this cold fluid varies from -1 to -1.1°C,

25 while at the same time, in the remaining part of the area being studied, the value varied from -0.04 to -0.97 °C (Figs. 6, 7).

This low-temperature anomaly was also observed in the middle horizon of the water column in under-ice conditions in previous years. Placing these stations on the tectonic map of the district, we discovered that all these anomalies coincide with the large faults formed by the Ust-Lena graben (Fig. 3). This connection is not evident at first glance,

30 however, but having obtained the possibility to measure the activity of the short-lived isotopes of radium in this water, we can shed light on the genesis of this anomaly.

3.3 Radium and Radon isotopes signals in the water column

35 The activities of the radium and radon isotopes and ^{224}Ra/ ^{223}Ra activity ratio have been measured in different horizons of the water column to determine the genesis of the thermohaline anomalies. The data are reported in Table 1. The distribution of ex^{224}Ra in the water samples ranged from 1.8 to 19 dpm/100L^{-1}, for ^{223}Ra from 0.14 to 0.65 dpm/100L^{-1} and for ex ^{222}Rn (excess ^{222}Rn, corrected for the ingrowth from ^{226}Ra) from 1 to 111×10^3 dpm/100L^{-1}, respectively (Table 1, Fig.8). The highest activities of ex^{224}Ra and ^{223}Ra (19 and 0.65 dpm/100L^{-1}) were detected in the bottom

40 horizons at station 1529, the exact same locations where the thermohaline anomalies were also detected. At this station, high values of radon activity were also registered, about 75×10^3 dpm/100L^{-1} (the highest activity of ^{222}Rn was recorded near st. 1529, at the st. 1504)(Table 1). The above-described low-temperature and salty plume at the surface and 6

meter horizons are thus also enriched in the short-lived radium and radon isotopes (Table 1, Fig.8, 9). In the river plume $ex^{224}Ra$, ^{223}Ra and $ex^{222}Rn$ activity was 9, 0.55 and 0.5×10^3 dpm/100L^{-1}, respectively. The activity of the short-lived radium and radon isotopes increases ($ex^{224}Ra=10.9$; $^{223}Ra=0.44$; $^{222}Rn=71\times10^3$ dpm/100L^{-1}) also near the Ice hummock (st. 1501) on the shallows of Cape Muostakh, a smooth hill of ice that forms under extreme weather

5 conditions during autumn ice formation. The activity ratios of $^{224}Ra/$ ^{223}Ra show here a range from 4.3 to 37.8 (Table 1).

In the "pure" ground water sampled from the two drilling wells, the activities of short-lived radium isotopes were $ex^{224}Ra=207$, $^{223}Ra=7.8$ dpm/100L^{-1} for wells ID15, and $ex^{224}Ra=224$, $^{223}Ra=8.5$ dpm/100L^{-1} for IID14, respectively. The activity ratio of $^{224}Ra/$ ^{223}Ra in the ground water was thus 26.5, close to the ratio found in the strongly enriched

10 bottom horizon of stations 1529 and 1520 (Table 1). This circumstance, and the fact that the highest activities of dissolved $ex^{224}Ra$, ^{223}Ra and $ex^{222}Rn$ isotopes were observed in the bottom horizon of the stations clearly points to submarine groundwater discharging indeed where the thermohaline anomalies were also discovered. At first view, such an isohaline structure may indicate the existence of vortex formations on this section, but with a very small depth (8 m not taking into account the ice), the leveling of the relief of the bottom, the stressed-out form and greater area of

15 the plumes in relation to the depth of the water (Fig. 5), as well as the data on temperature, short-lived radium and radon isotopes, suggests submarine groundwater discharge as a plausible mechanism consistent with these observations.

The signals described above that point to the existence of SGD near Stations 1529 and 1520 during the survey in winter (March-April 2015) find support also in the distribution of $ex^{224}Ra$ observed in the wider Delta area in

20 September 2013 (Fig. 10). The highest ^{224}Ra activity found during this summertime survey of the Lena Delta, 92.2 ± 1.9 dpm/100L^{-1} (Fig. 10), was found on Sept 1 at the bottom of Station 103 (Fig. 2), just 1.5 km South of Station 1529. This bottom water sample at 12m depth (salinity 15.9) also showed the highest activities of ^{226}Ra (31 ± 2 dpm/100L^{-1}) and ^{228}Ra (77 ± 4 dpm/100L^{-1}) observed during this cruise. Other high $ex^{224}Ra$ concentrations, in excess of 25 dpm/100L^{-1}, were observed at two more stations sampled on September 6 and 7: 69.1 ± 1.3 dpm/100L, was found at a

25 depth of 10m (bottom depth 12m, salinity 21.8) at Station Y (72°N/130°E, i.e. 23 km further north), and 43.4 ± 1.2 and 36.4 ± 1.2 dpm/100L^{-1} at depth of 2.5 and 5m, respectively (salinity 21.8 and 25.2, respectively), at shallow (6m water depth) Station 404 (73°N/130°E, i.e. 134 km further north). On this last day of the cruise, strong wind had caused very high turbidity at these shallow stations, and it is possible that resuspension of bottom sediments had released pore waters causing these high values. At these stations SGD may also have contributed to the release of ^{224}Ra, but we

30 cannot distinguish it from the possible role of resuspension. However, we interpret the coincidence of the very high $ex^{224}Ra$ concentration at the bottom of station 103 sampled during quiet weather conditions, with the observations at nearby station 1529 in winter 2015 as a strong argument that these were not due to resuspension but to SGD.

3.4 Ra isotope constraints on the origin of water masses

35

Figure 11a shows a theoretical mixing diagram, with the corners constituting the endmembers of the constituting water masses. Taken together, the data for the thermohaline structure, co-located with the high levels of activity of short-lived ^{224}Ra, ^{223}Ra and ^{222}Rn in these plumes, which are much higher than in the river water and in bottom waters elsewhere, leads to the conclusion that this thermohaline anomaly is the result of SGD.

40 The data in fig. 11 show the radium endmember concentrations in SW – seawater (bottom water), RW – river water (river plume) and TGW – transformed groundwater (the groundwater after mixing with seawater). We have separated

out two types of water that form because of the mixing of these three sources with each other (Table 1, Fig. 11): BW – brackish water and MGRSW – a mixture of ground, river and seawater.

GW – groundwater. These samples for end – member determination were obtained from sampling the two drilling wells, with the depth of the boreholes (the top of the bottom sediments is taken to be zero) being 18 and 15 m. The

5   lithological type of the sediments of these horizons was water-bearing sands. The $^{224}Ra/^{223}Ra$ activity ratio in the GW was 26.5. The ^{224}Ra activity was in the range of 207 to 224 dpm/100L^{-1}. The GWs is not represented on the graph due to a lack of salinity data.

RW – river water (river plume). This component is characterized by activities of ^{224}Ra, ^{223}Ra and ^{222}Rn that are higher than in SW, but lower than in TGW (Table 1, Fig. 11).

10   **SW – sea water (bottom water)**. This water mass ubiquitously has an almost unchanged activity of ^{224}Ra, ^{223}Ra and ^{222}Rn, and also in relation to $^{224}Ra/^{223}Ra$ itself. The $^{224}Ra/^{223}Ra$ activity ratio in the SW (bottom water) is higher than in the groundwater. This $^{224}Ra/^{223}Ra$ activity ratio is possibly explained by formation of a high density near – bottom nepheloid layer in the winter time from flocculation of humic substances and mineral particulates due to lack active mixing. Sinking thorium isotopes scavenged from surface horizons of the water column accumulate on the organic

15   and mineral particles in the bottom nepheloid horizon. Because of the much greater activity of ^{228}Th (half life = 1.9 years) with respect to ^{227}Th (half life = 18.9 days) after 5 months of wintertime the $^{228}Th/^{227}Th$ and $^{224}Ra/^{223}Ra$ ratios increases by ingrowth.

TGW – transformed groundwater. This component is formed by mixing of GW and bottom SW. As the result of this mixing, the highest activies of ^{224}Ra, ^{223}Ra and ^{222}Rn, were measured in this water; they are excellent tracers of

20   SGD (Moore and Arnold, 1996; Rama and Moore, 1996; Charette et al., 2008). The $^{224}Ra/^{223}Ra$ ratio in the discharge location was 29, which also points to a mixing of groundwater and bottom sea water (GW $^{224}Ra/^{223}Ra$=26; SW average of $^{224}Ra/^{223}Ra$=35). These waters were discovered at station 1529 in low-temperature fluid (Figs. 6, 7, 9). However, for the bottom horizon of stations 1504 and 1505, this is not a feature of SGD in this location, since first of all, the samples were taken 1 m from the bottom (see methods) and it was precisely at these stations that the low-temperature

25   fluid is closest to the bottom (Fig. 7), and secondly, the $^{224}Ra/^{223}Ra$ ratio at these stations is less than at station 1529, with similar values of salinity, which shows ^{224}Ra decay with time after SGD. The other situation is characteristic for the bottom horizon of station 1520, here SGD was not discovered either by temperature. However, ^{224}Ra, ^{223}Ra and ^{222}Rn activity and the $^{224}Ra/^{223}Ra$ ratio were comparable with station 1529 (Table 1, Fig. 8). Additionally, a shifting of isohalines was observed at station 1520 similar to that of station 1529, which points to mixing. This circumstance

30   can be explained by the fact that the source of the SGD is located close to station 1520, or that the discharge has a pulsating character.

BW – brackish water. This water is mainly found in the surface horizon formed as a result of mixing river water and seawater. It has a salinity range of 3.8 to 11.9, with large dispersion of ^{224}Ra activity (6.9 – 1.8 dpm/100L^{-1}) and $^{224}Ra/^{223}Ra$ ratio (4.3 – 36.4).

35   **MGRSW – mixture of GW, RW and SW.** These points lie in the central part of the mixing triangle (Fig. 11a) and in the middle of the trend line (Fig. 11b), and are characterized by high or similar ^{224}Ra and ^{223}Ra activity in comparison with RW and SW. Moreover, the salinity in MGRSW is less than in SW and TGW. Among these are the points in the plume of the surface horizon of station 1520 (^{224}Ra activity is 1.3 times higher than the ^{224}Ra activity of the surface horizon of the neighboring stations 1529 and 1504), and the waters on the periphery of the ice hummocks (called

40   *stamukha* in Russian) on the shallows around Cape Muostakh. The activity ratio of $^{224}Ra/^{223}Ra$ varies here from 18 to 29.

3.5 Mechanisms of submarine groundwater discharge

3.5.1 Discharge of the subpermafrost water

5

The study area is located in a permafrost region, which complicates not only discharge, but also recharge of the groundwater. Therefore, in our case, the only means of recharging is open taliks. Such terrain features facilitate interaction of suprapermafrost water with subpermafrost water, which forms in the valleys of large rivers, by lakes and in fault zones. In the river watershed, the suprapermafrost water collects from surrounding slopes (Fig.12a)

10 (Pinneker, 1983, Romanovskii, 1983). In the current study area, one of the main sources of groundwater recharge may be the large Lena River, which flows several hundred kilometers from our SGD, along the other side of the Kharaulakh Ridge (Fig. 12b).

It is known that open taliks exist in the river bed of the Lena River (Antonov, 1987, Semiletov et. al., 2000) in the area of the West-Verkhoyan Fault (Fig. 12b), hydraulically connected by fissures and faults with groundwater of the

15 entire hydrogeological massif (Fig. 12a). Additionally, researchers have noted that the level of water arriving in the Lena River Delta is higher than that measured at the outlet of the river (Bolshiyanov et al., 2013; Fedorova et. al., 2015). This difference in elevation is explained by the complex hydrographic layout of the delta and peculiarities of delta geological and geomorphological structure, and it creates a pressure gradient for submarine groundwater discharge.

20 The waters of the open taliks of large rivers and lakes penetrate through the permafrost and mix with the cryogenic groundwater. This water was formed as the result of multi-year freezing of rocks and the simultaneous concentration of salts (Pinneker, 1983; Romanovskii, 1983), resulting in total dissolved solids in the cryogenic groundwater from 1×10^4 to 30×10^4 mg/L and a temperature from 0 to -12 °C. In the Kharaulakh hydrogeological massif, the thickness of the cryogenic groundwater reaches 300-400 meters, with a thickness of the permafrost of 500-700 meters

25 (Romanovskii, 1983) (Fig. 12a). In the end, the cryogenic groundwater contributes to the cold and salty groundwater (GW) which is released as SGD, and which, after mixing with fresh water from rivers and lakes, and with bottom seawater, transforms into the cold (about -1°C) and saline (salinity 22) TGW. Taken together, the scheme of water masses mixing after SGD is outlined in figure 12c.

The study area is part of the Kharaulakh hydrogeological massif (North of Verkhoyansk Fold) which is complicated

30 by listric faults along the coastline (Romanovskii, 1983, Imaev, et. al., 2004) (Fig. 3, 4). For lithified rocks of hydrogeological massif the permeability and water-bearing capacity is governed by the presence of fissures, faults, and pores (Pinneker, 1983, Romanovskiy, 1983). Usually the young active faults are the most crushed and broken (Sherard, et al., 1974), therefore, in our case, the Neogene-Quaternary faults along the coastline of the Buor-Khaya Gulf have favorable conditions for the transport of under-pressure subpermafrost water. The lack of permafrost over

35 the fault zones removes the last obstacle to the path of flowing groundwater before it is discharged into the water column of the Buor-Khaya Gulf. The small shift in location of the SGD to the east relative to the fault line is possibly caused by the presence of fine sediments stratum (confining bed), which we discovered by TEM on the top of the footwall of the listric faults (Fig. 12c). The fact that the summertime and wintertime SGD springs were found on a line parallel to the fault once again points to the connection between the tectonogenic talik and the SGD (Fig. 4).

40 The probable cause of the SGD being located precisely in this sector of the fault may be that here the listric fault crosses another fault with unknown kinematics (Fig. 4a). It is known that where two faults of different orientations meet or cross each other a larger part of the rock masses suffers from increased crushing or jointing (Selmer-Olsen,

1964), and this in turn creates favorable conditions for rising groundwaters. The region more westerly of our SGD sites has a similar tectonic structure (fault crossing). However, there are no features of an SGD, which may be explained by the following. On the surface of this area is categorized as vast shoals, which for the greater part of the year is covered by fast ice and ice hummock frizzing with sediments. Furthermore, it was flooded much later by the transgression of the sea, and possibly these shoals arose exclusively due to thermal abrasion already after the time of marine transgression, which gives grounds to presume that the permafrost starts already at shallow depths below the surface sediments and thus hinders SGD (Fig. 12a). In addition, it is likely that the fine sediments stratum (confining bed) observed by TEM at the geophysical station 2 is widespread in this area.

3.5.2 Cryogenic squeezing out of brine (CSB) and water-soluble salts

Besides the fluid and river plume examined above, there was one more place in the area that was studied, which also had high activities of the isotopes ^{224}Ra, ^{223}Ra and ^{222}Rn. The radium and radon activities were significantly higher than in the river plume on the periphery of the ice hummocks, the shoals of Cape Muostakh (Station 1501). Moreover, the salinity of the entire column exceeded 12 (Fig. 6), and furthermore, this point was located in the region impacted by drainage of the Lena River (Charkin et. al., 2011) and far apart from our under pressure SGD. On the graph of the dependency of ^{224}Ra and ^{224}Ra/^{223}Ra on salinity (Fig. 13), this point lays in the region of the MGRSW, which is the mixing of river, sea and groundwater. Taken together this phenomenon is likely the result of cryogenic squeezing out of brine (CSB) and water-soluble salts due to a compression and crystallization effect from the ice formation zone into the warmer unfrozen parts of the sediments. This phenomenon has been described in permafrost on land (Tyutyunov, 1966, Baker, and Osterkamp, 1989, Shepelev and Sannikova, 2001), and we may here have noted it for the first time in the sea bottom sediments.

During the autumn-winter formation of the fast ice, huge areas of the shoals of the Buor-Khaya Gulf freeze with ice. As the result of the freezing of water-bearing sands, the cryogenic squeezing of brine (CSB) and water soluble salts occurs in the part which has not frozen.

Figure 13 shows the mechanism of this SGD formation. Under the impact of a hydraulic piston, the water is confined by the bed of clay (documented in drill borehole 4D-12 (Figs. 4a, b), which is located together with the cryogenically confining bed of submarine permafrost. As a result, the brine flows along the path of least resistance and enters into the water column of the adjacent body of water and starts mixing.

Despite the large area of the shallows and bars in the Buor-Khaya Gulf, we have not detected the strong influence of this process on the thermohaline structure of the investigated area. This phenomenon is observed at the place of direct contact between the ice hummock and bottom sediments. The coast orography also is an important factor. The location of the discovered phenomenon is closed from the main water flow of riverine waters by a spit of land which restricted removal of discharged groundwater (Figs. 2, 4, 6).

4 Conclusions

The features and nature of subpermafrost groundwater discharge in the Siberian Arctic seas depend on thermal state of the permafrost as well as the geological and tectonic structure of the shelf. The geological prerequisites for subpermafrost groundwater discharge include presence of lithological conditions (sands, gravel, cracks and fissures in rocks) and channel ("taliks") between the subpermafrost groundwater (confined aquifer) and the marine water

column. From the tectonic position, the most favorable conditions for the discharge of pressurized subpermafrost groundwater are formed in the rifting of active fault zones, especially at the locations of fault crossings. Since, first, there is an increased crushing or jointing of rock masses, which is favorable for the uprising transport of groundwater, and secondly, the impact of endogenous heat flux is increased, which thaws the permafrost.

5   The cryogenic conditions formed in the bottom sediments of shoals, where newly frozen sediments function as a hydraulic piston pushing interstitial brine and salt into the water column. However, we consider the significance of such groundwater to be less significant in comparison with the mechanism of under-pressure ground water to overall production.

This study is the first to directly observe submarine groundwater discharge along the Eurasian Arctic margin. It
10   introduces a mechanistic context for this process. Future studies should seek to expand on the multi-proxy approach to constrain the quantitative significance of this transport vector not only for freshwater discharge but also for associated old carbon released from the permafrost system.

Data availability

15   All data are available in Table 1, as well as Supplementary Tables S1 and S2.

References

30

Antonov, V. S.: Mouth area of the Lena river (hydrological sketch), Leningrad, Hydrometizdat, 1–107, 1987 (in Russian).

Anderson, B., Bryant, I., L˜ulig, M., Spies, B., and Helbig, K.: Oilfield anisotropy: Its origins and electrical characteristics, Oilfield Rev., 6(4), 48–56, 1994.
35   Bisson, R.A.: Space-age integrated exploration and treatment of renewable regional sources of pristine ground water in fractured rock megawatersheds, Desalination, 99, 257-273, 1994.

Burnett, W. C., Peterson, C. R., Moore, W. S., and De Olivera J.: Radon and radium isotopes as tracers of submarine groundwater discharge—results from the Ubatuba Brazil SGD assessment intercomparison, Estuar. Coast. Shelf Sci., 76, 501–511, doi:10.1016/j.ecss.2007.07.027, 2008.

Burt, W.J.; Thomas, H.; Pätsch, J.; Omar, A.; Schrum, C.; Daewel, U.; Brenner, H.; de Baar, H.J.W.: Radium isotopes as a tracer of sediment-water column exchange in the North Sea, Global Biogeochem. Cycles, 28(8), 786–804. dx.doi.org/10.1002/2014GB004825, 2014.

Bolshiyanov, D. Yu., Makarov, A. S., Schneider, V., and Stoof, G.: Origin and development of the Lena River Delta,
5   AARI, St. Petersburg, 1-267, 2013 (in Russian).

Baker, G. C., and T. E. Osterkamp.: Salt distribution during freezing of saline sand columns at constant rates, Water Resour. Res., 25, 1825–1831, 1989.

Carmack, E. C.: The Arctic Ocean's freshwater budget: Sources, storage and export, in The Freshwater Budget of the Arctic Ocean, edited by E. L. Lewis et al., Springer, New York. 91– 126, 2000.

10   Charkin, A.N., Dudarev O.V., Semiletov I.P., Kruhmalev A.V., Vonk J.E., Sánchez-García L., Karlsson E., and Gustafsson Ö.: Seasonal and interannual variability of sedimentation and organic matter distribution in the Buor-Khaya Gulf: the primary recipient of input of Lena River and coastal erosion in the Southeast Laptev Sea, Biogeosciences, 8, 2581–2594, doi:10.5194/bg-8-2581-2011, 2011.

Charkin, A. N., Dudarev, O. V., Shakhova, N. E., Semiletov, I. P., Pipko, I. I., Pugach, S. P. and Sergienko, V. I.:
15   Peculiarities of the formation of suspended particulate matter fields in the Eastern Arctic seas. Doklady Earth Sciences, 462(2), 626-630. doi: 10.1134/S1028334X15060100, 2015.

Charette, M. A., Gonneea, M. E., Morris, P., Statham, P., Fones, G., Planquette, H. I., and Salter, A.: Radium isotopes as tracers of iron sources fueling a Southern Ocean phytoplankton bloom, Deep-Sea Res. II, 54, 1989–1998, 2007.

Charette, M.A., Moore, W.S., Burnett, W.C.: Uranium- and thorium-series nuclides as tracers of submarine
20   groundwater discharge, In: Krishnaswami, S., Cochran, J.K. (Eds.), Radioactivity in the Environment. U–Th Series Nuclides in Aquatic Systems, 13, 155–191, 2008.

Charette, M. A., Breier, C. F., Henderson, P. B., Pike, S. M., Rypina, I. I., Jayne, S. R., and Buesseler, K. O.: Radium-based estimates of cesium isotope transport and total direct ocean discharges from the Fukushima Nuclear Power Plant accident, Biogeosciences, 10, 2159–2167, doi:10.5194/bg-10-2159-2013, 2013.

25   Charette, M. A., Splivallo R., Herbold C., Bollinger M. S., and Moore W. S.: Salt marsh submarine groundwater discharge as traced by radium isotopes, Mar. Chem., 84, 113–121, 2003.

Drachev, S.S., Savostin, L.A., Groshev, V.G., Bruni, I.E.: Structure and geology of the continental shelf of the Laptev Sea, Eastern Russian Arctic, Tectonophysics, 298, 357-393, 1998.

Drachev, S. S., Johnson, G. L., Laxon, S. W., McAdoo, D. C., and Kassens, H.: Main structural elements of Eastern
30   Russian Arctic continental margin derived from satellite gravity and multichannel seismic reflection data, in: Land-Ocean Systems in the Siberian Arctic: Dynamics and History, edited by: H. Kassens, H., Bauch, H. A., Dimitrenko, I. A., et al., Springer, 667–692, 1999.

Dimova, N.T., Paytan, A., Kessler, J.D., Sparrow, K.J., Garcia-Tigreros Kodovska, F., Lecher, A.L., Murray, J., Tulaczyk, S.M.: Current magnitude and mechanisms of groundwater discharge in the Arctic: case study from Alaska,
35   Environ. Sci. Technol., 49, 12036–12043, http://dx.doi.org/10.1021/acs.est.5b02215, 2015.

Dulaiova, H., Burnett, W.C., Chanton, J.P., Moore, W.S., Bokuniewicz, H.J., Charette, M.A., Sholkovitz, E.: Assessment of groundwater discharge into West Neck Bay, New York, via natural tracers, Continental Shelf Research, 26, 16, 1971–1983, 2006.

Franke, D., Hinz, K., Oncken, O.: The Laptev Sea Rift, Marine and Petroleum Geology, 18, 1083-1127, 2001.

40   Fedorova, I. , Chetverova, A. , Bolshiyanov, D. , Makarov, A. , Boike, J. , Heim, B. , Morgenstern, A. , Overduin, P. P. , Wegner, C. , Kashina, V. , Eulenburg, A. , Dobrotina, E. , and Sidorina, I.: Lena Delta hydrology and geochemistry:

long-term hydrological data and recent field observations , Biogeosciences, 12, 2, 345-363, doi: 10.5194/bg-12-345-2015, 2015.

Gordeev, V. V., Martin, J. M., Sidorov, I. S., and Sidorova, M. V.: A reassessment of the Eurasian river input of water sediment, major elements, and nutrients to the Arctic Ocean, American Journal of Science, 296, 664–691, 1996.

5 General hydrogeology by E. V. Pinneker (Ed.), Cambridge University Press, 1-141, Translated from Russian by D. E. Howard and J. C. Harvey, 1983.

Gu, H., Moore, W. S., Zhang, L., Du, J., and Zhang, J.: Using radium isotopes to estimate the residence time and the contribution of submarine groundwater discharge (SGD) in the Changjiang effluent plume, East China Sea, Cont. Shelf Res., 35, 95–107, 2012.

10 Gonçalves-Araujo, R., Stedmon, C.A., Heim, B., Dubinenkov, I., Kraberg, A., Moiseev, D., Bracher, A.,. From Fresh to Marine Waters: Characterization and Fate of Dissolved Organic Matter in the Lena River Delta Region, Siberia. Front. Mar.Sci.2:108. doi: 10.3389/fmars.2015.00108, 2015.

Hathaway, J.C., Poag, C.W., Valentine, P.C., Miller, R.E., Schultz, D.M., Manheim, F.T., Kohout, F.A., Bothner, M.H., Sangrey, D.A., US Geological Survey core drilling on the Atlantic shelf, Science, 206, 515–527, 1979.

15 Hancock, G. J., Webster, I. T., and Stieglitz, T. C.: Horizontal mixing of Great Barrier Reef waters: Offshore diffusivity determined from radium isotope distribution, J. Geophys. Res., 111, doi:10.1029/2006JC003608, 2006.

Hougham, A. L., and S. B. Moran.: Water mass ages of coastal ponds estimated using ^{223}Ra and ^{224}Ra as tracers. Mar. Chem., 105, 194 – 207, 2007.

Imaev V.S., Imaeva L.P., Kozmin B.M. The Oceanic and continental Rifts of the North-Eastern Asia (seismotectonic
20 analysis), Lithosphere, 4, 44-61, 2004 (in Russian).

Kohout, F.A., Meisler, H., Meyer, F.W., Johnston, R.H., Leve, G.W., and Wait, R.L.: Hydrogeology of the Atlantic continental margin, In The Geology of North America, I–2, The Atlantic Continental Margin, ed. R.E. Sheridan and J.A. Grow, Boulder, Colorado: Geological Society of America, 463–480, 1988.

Kadko, D., Pickart, R. S., Mathis, J.: Age characteristics of a shelf-break eddy in the western Arctic and implications
25 for shelf-basin exchange, Journal of Geophysical Research, 113, C02018, doi:10.1029/2007JC004429, 2008.

Kadko, D., and Aagaard, K.: Glimpses of Arctic Ocean shelf-basin interaction from submarine-borne radium sampling, Deep Sea Res., I 56, 32–40, 2009.

Keller G.V., and Frischknecht F.C.: Electrical methods in geophysical prospecting, Pergamon Press Inc., Oxford, 1-519, 1966.

30 Koshurnikov, A. V., Tumskoy, V. E., Shakhova, N. E., Sergienko, V. I., Dudarev, O. V., Gunar, A. Y.: The first ever application of electromagnetic sounding for mapping the submarine permafrost table on the Laptev Sea shelf. Doklady Earth Sciences, 469(2), 860-863. DOI: 10.1134/S1028334X16080110, 2016.

Lecher, A.L., Kessler, J., Sparrow, K., Garcia-Tigreros Kodovska, F., Dimova, N., Murray, J., Tulaczyk, S., Paytan, A.: Methane transport through submarine groundwater discharge to the north Pacific and Arctic Ocean at two Alaskan
35 sites, Limnol. Oceanogr., ttp://dx.doi.org/10.1002/lno.10118, 2015.

McClelland, J.W., De´ry, S. J., Peterson, B. J., Holmes, R. M., and Wood, E. F.: A panarctic evaluation of changes in river discharge during the latter half of the 20th century, Geophys. Res. Lett., 33, L06715, doi:10.1029/2006GL025753, 2006.

Macdonald R.W., Anderson L.G., Christensen J.P., Miller L.A., Semiletov I.P., and R. Stein: The Arctic Ocean:
40 budgets and fluxes, In "Carbon and Nutrient Fluxes in Continental Margins: A Global Synthesis," Edited by K.-K. Liu, L. Atkinson, R. Quinones, L. Talaue-McManus, Springer-Verlag, 291-303, 2008.

Moore, W. S.: Sampling ^{228}Ra in the deep ocean. Deep-Sea Res, Oceanogr. Abstr., 23, 647-651, 1976.

Moore, W.S.: The subterranean estuary: a reaction zone of ground water and sea water, Marine Chem., 65, 111–26, 1999.

Moore, W.S. 1996. Large groundwater inputs to coastal waters revealed by [226]Ra enrichments. Nature 380:612–14

Moore, W.S.: Determining coastal mixing rates using radium isotopes, Cont. Shelf Res., 20, 1993–2007, 2000a.

5   Moore, W.S.: Ages of continental shelf waters determined from [223]Ra and [224]Ra, J. Geophys. Res. Oceans, 105, 22, 117–222, 2000b.

Moore, W.S., and Krest, J.: Distribution of [223]Ra and [224]Ra in the plumes of the Mississippi and Atchafalaya Rivers and the Gulf of Mexico, Mar. Chem., 86, 105–119, 2004.

Moore, W.S, Blanton, J.O, Joye, S.B.: Estimates of flushing times, submarine groundwater discharge, and nutrient

10   fluxes to Okatee Estuary, South Carolina, J. Geophys. Res.-Oceans, 111, doi: 10.1029/2005jc003041, 2006.

Moore, W.S., and Arnold, R., Measurement of [223]Ra and [224]Ra in coastal waters using delayed coincidence counter, J. Geophys. Res., 101: 1321–1329. 1996.

Moore, W.S., and de Oliveira, J.: Determination of residence time and mixing processes of the Ubatuba, Brazil, inner shelf waters using natural Ra isotopes. Estuar. Coast. Shelf S., 76, 512-521, doi:10.1016/j.ecss.2007.07.042, 2008.

15   Moore, W.S., Cai, P.: Calibration of RaDeCC systems for [223]Ra measurements, Mar. Chem., 156, 130–137, 2013.

Maintenance manual Radiometer RRA-01M-03, Measurement routine of volumetric activity of radon in water samples, concurrently by VNIIFTRI (Rapid analysis), Moscow, Russia: LLC "NTM-protection", 2004. p.1-15.

Nicolsky, D., and Shakhova, N.: Modeling sub-sea permafrost in the East-Siberian Arctic Shelf: the Dmitry Laptev Strait, Environ Res. Lett., 5, doi:10.1088/1748-9326/5/1/015006, 2010.

20   Nicolsky, D.J., Romanovsky, V.E., Romanovskii, N., Kholodov, A.L., Shakhova, N.E., and Semiletov, I.: Modeling sub-sea permafrost in the East Siberian Arctic Shelf: The Laptev Sea Region, Journal of Geophysical Research, doi:10.1029/2012JF002358, 2012.

Peterson, B. J., R. M. Holmes, J. W. McClelland, C. J. Vörösmarty, R. B. Lammers, A. I. Shiklomanov, I. A., and Rahmstorf, S.: Increasing river discharge to the Arctic Ocean, Science, 298, 2171– 2173, 2002.

25   Palacky, G. J.: Resistivity characteristics of geologic targets, in Investigations in Geophysics, 3, Electromagnetic methods in applied geophysics-theory, 1, edited by M. N. Nabighian, Soc. Expl. Geophys., 53–129, 1988.

Rama, and Moore, W.S.: Using the radium quartet for evaluating groundwater input and water exchange in salt marshes, Geochim. Cosmochim. Acta, 60, 4645–4652, 1996.

Rutgers van der Loeff, M. M., Key, R. M., Scholten, J. C., Bauch, D., and Michel, A.: [228]Ra as a tracer for shelf water

30   in the Arctic Ocean, Deep-Sea Res., II 42, 1533-1553, 1995.

Rutgers van der Loeff, M., Kuhne, S., Wahsner, M., Holtzen, H., Frank, M., Ekwurzel, B., Mensch, M., and Rachold, V.: [228]Ra and [226]Ra in the Kara and Laptev seas, Cont. Shelf Res., 23, 113-124, 2003.

Rutgers van der Loeff, M., Cai, P., Stimac, I., Bauch, D., Hanfland, C., Roeske, T., and Moran, S. B.: Shelf-basin exchange times of Arctic surface waters estimated from [228]Th/[228]Ra disequilibrium, J. Geophys. Res. Oceans, 117,

35   C3, C03024, 2012.

Rapaglia, J., Ferrarin, C., Zaggia, L., Moore, W. S., Umgiesser, G., Garcia-Solsona, E., Garcia-Orellana, J., and Masqué P.: Investigation of residence time and groundwater flux in Venice Lagoon: Comparing radium isotope and hydrodynamical models, J. Environ. Radioact., 101, 7, 571–581, 2010.

Romanovskii N.N.: Groundwater in the permafrost zone, Lomonosov Moscow State University Press, 1-231, 1983

40   (in Russian).

Romanovskii, N. N., Hubberten, H. W., Gavrilov, A. V., Eliseeva, A. A., and Tipenko, G. S.: Offshore permafrost and gas hydrate stability zone on the shelf of East Siberian Seas, Geo-Marine Letters, 25, 2-3, 167-182, 2005.

Sánchez-García L., Vonk J.E., Charkin A.N., Kosmach D., Dudarev O.V., Semiletov, I., Ö. Gustafsson: Characterisation of Three Regimes of Collapsing Arctic Ice Complex Deposits on the SE Laptev Sea Coast using Biomarkers and Dual Carbon Isotopes, Permafrost and Periglac. Process, Vol. 25, p. 172–183, 2014.

Savelieva, N. I., Semiletov, I. P., Vasilevskaya, L. N., and Pugach. S. P.: A climate shift inseasonal values of meteorological and hydrological parameters for northeastern Asia. Progress in Oceanography 47, 279 –297, 2000.

Semiletov, I.P., Pipko, I.I., Pivovarov, N.Ya., Popov, V.V., Zimov, S.A., Voropaev, Yu.V. and Daviodov S.P.: Atmospheric carbon emissions from northern lakes: a factor of global significance, Atmopheric. Environment, 30, 1657-1671, 1996.

Semiletov, I.P. On aquatic sources and sinks of CO_2 and CH_4 in the Polar Regions, *J. Atmos. Sci.*, *56,* 286-306, 1999.

Semiletov, I. P., Savelieva, N. I., Weller, G. E., Pipko, I. I., Pugach, S. P., Gukov, A. Yu., and Vasilevskaya, L. N.: The dispersion of Siberian river flows into coastal waters: Meteorological, hydrological, and hydrochemical aspects. In The Freshwater budget of the Arctic Ocean: Proceedings of the NATO Advanced Research Workshop, Tallinn, Estonia, 27 April-1 May 1998, eds. E. L. Lewis, E. P. Jones, P. Lemke, T. D. Prowse, and P. Wadhams, Dordrect: Kluwer Press., 323–366, 2000.

Semiletov, I., I.I. Pipko, I.A. Repina, and N. Shakhova: Carbonate dynamics and carbon dioxide fluxes across the atmosphere-ice-water interfaces in the Arctic Ocean Pacific sector of the Arctic, Journal of Marine Systems, 66 (1-4), 204-226, 2007.

Semiletov, I.P., and Gustafsson Ö.: East Siberian Shelf Study alleviates scarcity of observations, EOS Trans. AGU, 90(17), 145, doi:10.1029/2009EO170001, 2009.

Semiletov I.P., Shakhova N. E., Sergienko V.I., Pipko I.I., and O. Dudarev: On Carbon Transport and Fate in the East Siberian Arctic Land-Shelf-Atmosphere System, Environment Research Letters, 7, doi:10.1088/1748-9326/7/1/015201, 2012.

Semiletov I.P., Shakhova N. E., Pipko I.I., Pugach S.P., Charkin A.N., Dudarev O.V., Kosmach D.A., and S. Nishino: Space-time dynamics of carbon stocks and environmental parameters related to carbon dioxide emissions in the Buor-Khaya Bay of the Laptev Sea, Biogeosciences, 10, 5977-5996; doi:10.5194/bg-10-5977-2013, 2013.

Semiletov I., Pipko I., Gustafsson O., Anderson L., Sergienko V., Pugach S., Dudarev O., Charkin A., Broder L., Andersson A., Spivak E., and N. Shakhova: Acidification of the East Siberian Arctic Shelf waters through addition of freshwater and terrestrial carbon, Nature Geosciences, April 18 2016, doi:10.1038/NEGO 2695, 2016.

Sherard, J.L., Cluff, L.S., and Allen, C.R.: Potentially active faults in dam foundations, Geotechnique, 24, 367-428, 1974.

Selmer-Olsen R.: Geology and engineering geology, Tapir, Trondheim, Norway, 1-409, 1964.

Serreze, M. C., Barrett, A. P., Slater, A. G., Woodgate, R. A., Aagaard, K., Lammers, R. B., Steele, M., Moritz, R., Meredith, M., and Lee, C. M..: The large-scale freshwater cycle of the Arctic, J. Geophys. Res., 111, C11010, doi:10.1029/2005JC003424, 2006.

Shakhova, N. and Semiletov I.: Methane release and coastal environment in the East Siberian Arctic shelf, Journal of Marine Systems 66 (1-4), 227-243, 2007.

Shakhova N.E., Nicolsky D., and Semiletov, I. P.: On the current state of sub-sea permafrost in the East-Siberian Shelf testing of modeling results by observational data. Transactions of Russian Academy of Sciences, 429, 5, 2009 (translated in English by Springer).

Shakhova, N., Semiletov, I., Sergienko, V., Lobkovsky, L., Yusupov, V., Salyuk, A., Salomatin, A., Chernykh, D., Kosmach, D., Panteleev, G., Nicolsky, D., Samarkin, V., Joye, S., Charkin, A., Dudarev, O., Meluzov, A., Gustafsson

O.: The East Siberian Arctic Shelf: towards further assessment of permafrost-related methane fluxes and role of sea ice, Phil. Trans. R. Soc. A, 373, 20140451. http://dx.doi.org/10.1098/rsta.2014.0451, 2015

Shakhova, N., Semiletov, I., Leifer, I., , Sergienko, V., Salyuk, A., Kosmach, D., Chernikh D., Stubbs Ch., Nicolsky D., Tumskoy V., and Gustafsson, O.: Ebullition and storm-induced methane release from the East Siberian Arctic
5   Shelf, Nature Geosciences, January 2014, 7, 1, 64-70, 2014.

Shakhova N., Semiletov I., Leifer I., Rekant P., Salyuk A., and Kosmach, D.: Geochemical and geophysical evidence of methane release from the inner East Siberian Shelf, Journal Geophys. Res 115, doi:10.1029/2009JC005602, 2010.

Shepelev V.V., and Sannikova A.V.: The regime of suprapermafrost water in the Active Layer, Yakutsk Area, Proc. Of the 7 Intern. Symp. Of Thermal Eng. And Sci. for Cold Regions, Seoul, Korea, 139-143, 2001.

10   Shiklomanov, I. A., Shiklomanov, A. I., Lammers, R. B., Vörösmarty, C. J., Peterson, B. J., and Fekete, B.: The dynamics of river water inflow to the Arctic Ocean. In The freshwater budget of the Arctic Ocean: Proceedings of the NATO Advanced Research Workshop, Tallinn, Estonia, 27 April–1 May 1998, eds. E. L. Lewis, E. P. Jones, P. Lemke, T. D.Prowse, and P. Wadhams, Dordrect: Kluwer Press, 281–296, 2000.

Schirrmeister, L., Grosse, G., Kunitsky, V., Magens, D., Meyer, H., Dereviagin, A., Kuznetsova, T., Andreev, A.,
15   Babiy, O., Kienast, F., Grigoriev, M., Overduin, P., Preusser, F.: Periglacial landscape evolution and environmental changes of Arctic lowland areas for the last 60 000 years western Laptev Sea coast, Cape Mamontov Klyk, Polar Research, 27, 249-272, doi:10.1111/j.1751-8369.2008.00067.x, 2008.

Stepanov V.E. Egorova S.E. Radon emanation characteristics in Central Yakutia" International symposium "Euro-Eco-2014" program abstracts 1. Hannover, Germany: European Scientific Society, p. 50-51, 2014.

20   Tyutyunov V.A.: Phase transformations of water in soils and the nature of migration and heaving, First ICOP Proceedings - Lafayette, Indiana, 234-238, 1966.

Vörösmarty, C. J., Hinzman, L. D., Peterson, B. J., Bromwich, D. H., Hamilton, L. C., Morison, J., Romanovsky, V. E., Sturm, M. and Webb R. S.: The Hydrologic Cycle and its Role in Arctic and Global Environmental Change: A Rationale and Strategy for Synthesis Study. Fairbanks, Alaska: Arctic Research Consortium of the U.S., 1-84,
25   http://scitechdaily.com/images/New-NASA-Estimates-of-Liquid-Assets.jpg, 2001.

Velicogna, I., Tong, J., Zhang, T., and Kimball, J. S.: Increasing subsurface water storage in discontinuous permafrost areas of the Lena River basin, Eurasia, detected from GRACE, Geophys. Res. Lett., 39, L09403, 1-5, doi:10.1029/2012GL051623, 2012.

Vonk, J., Sánchez-García, L., van Dongen, B., Alling, V., Kosmach, D., Charkin, A.N., Semiletov, I., Dudarev, O.
30   Shakhova, N., Roos, P., Eglinton, T., Andersson, A. and Gustafsson, Ö.: Activation of old carbon by erosion of coastal and subsea permafrost in Arctic Siberia. Nature, doi:10.1038/nature11392, 2012.

Vonk, J.E., Semiletov, I.P., Dudarev, O.V., Eglinton, T.I., Andersson, A., Shakhova, N., Charkin, A., Heim, B., Gustafsson, Ö.: Preferential burial of permafrost derived organic carbon in Siberian-Arctic shelf waters, J. Geophys. Res., Vol. 119, N 12, P. 8410-8421, 2014.

35   Ward, S. H.: Geotechnical and Environmental Geophysics, chapter Resistivity and Induced Polarization Methods, Investigations in Geophysics, 5, Soc. Expl. Geophys, 147–189, 1990.

Walvoord, M. A., and Striegl R. G.: Increased groundwater to stream discharge from permafrost thawing in the Yukon River basin: Potential impacts on lateral export of carbon and nitrogen, Geophys. Res. Lett., 34, L12402, doi:10.1029/2007GL030216, 2007.

40   Yang, D., Kane, D. L., Hinzman, L., Zhang, X., Zhang, T., and Ye, H.: Siberian Lena River hydrologic regime and recent change, J. Geophys. Res., 107, D23, 46-94, doi:10.1029/2002JD002542, 2002.

Table 1. **Salinity, temperature (°C), activities of short-lived Radium and Radon isotopes (dpm/100L^{-1}), ^{224}Ra/^{223}Ra activity ratio at the sampling sites in the western part of the Buor-Khaya Gulf (Laptev Sea) during the wintertime season.**

| Station ID	Horizon	Water type	Salinity	Temperature	ex ^{224}Ra	^{223}Ra	224/223 AR	ex ^{222}Rn
ID15	18 m	GW	-*	-*	207 ± 3.9	7.8 ± 0.65	26.5	-*
IID14	15 m	GW	-	-	224 ± 2.5	8.5 ± 0.48	26.4	-
GW average (n=2)			-	-	215 ± 3.2	8.15 ± 0.56	26.45	-
Standard deviation			-	-	12	0.49	0.07	-
1529	bottom	TGW	22.1	- 1.01	19 ± 0.44	0.65 ± 0.06	29.2	75×10^3 ± 300
1520	bottom	TGW	22.2	- 0.96	16.8 ± 0.55	0.58 ± 0.07	29	66×10^3 ± 265
1504	bottom	TGW	22.7	- 1	14.5 ± 0.55	0.75 ± 0.10	19.3	111×10^3 ± 445
1505	bottom	TGW	22.1	- 0.97	14.3 ± 0.48	0.62 ± 0.08	23.1	-
1507	6 m	TGW	20.9	- 0.98	8.2 ± 0.25	0.34 ± 0.04	24.1	24×10^3 ± 98
TGW average (n=5)			22	-0.98	14.6 ± 0.45	0.59 ± 0.08	24.9	64×10^3 ± 277
Standard deviation			0.66	0.02	4.04	0.15	4.2	355
1501	mid	MRGSW	12.4	- 0.57	10.9 ± 0.39	0.44 ± 0.06	24.7	71×10^3 ± 94
1520	surface	MRGSW	11.5	- 0.67	7.6 ± 0.38	0.42 ± 0.07	18	-
1508	surface	MRGSW	10.9	- 0.58	7.3 ± 0.34	0.25 ± 0.05	29.2	-
1529	6 m	MRGSW	17.8	- 1	5.4 ± 0.34	0.21 ± 0.04	26.1	-
MRGSW average (n=4)			13.1	-0.71	7.8 ± 0.36	0.33 ± 0.05	24.5	-
Standard deviation			3.16	0.2	2.28	0.12	4.72	-
1502	mid	RW	0.98	- 0.06	9 ± 0.37	0.55 ± 0.07	16.4	0.5×10^3 ± 2
1515	surface	RW	1.6	- 0.09	6.3 ± 0.35	0.4 ± 0.07	15.7	-
1531	mid	RW	1.73	- 0.08	1.8 ± 0.37	0.42 ± 0.08	4.3	-
RW average (n=3)			1.4	-0.07	5.7 ± 0.36	0.45 ± 0.07	12.1	-
Standard deviation			0.4	0.02	3.6	0.08	6.8	-
1530	surface	BW	3.8	- 0.2	4.3 ± 0.35	0.15 ± 0.05	28.6	-
1503	mid	BW	4.1	- 0.22	5.1 ± 0.45	0.14 ± 0.04	36.4	0.8×10^3 ± 3
1532	mid	BW	6.7	- 0.2	4.7 ± 0.9	0.28 ± 0.11	16.7	-
1514	surface	BW	7.1	- 0.39	5.2 ± 0.42	0.19 ± 0.05	27.3	0.2×10^3 ± 0.9
1507	surface	BW	7.8	- 0.43	5.9 ± 0.36	0.26 ± 0.05	22.7	0.3×10^3 ± 1
1506	mid	BW	8.5	- 0.4	5.6 ± 0.24	0.44 ± 0.06	12.7	-
1504	surface	BW	9.4	- 0.53	5.7 ± 0.42	0.22 ± 0.05	25.9	-
1509	mid	BW	9.6	- 0.51	6.9 ± 0.32	0.28 ± 0.05	24.6	0.2×10^3 ± 0.9
1505	surface	BW	9.8	- 0.54	6.2 ± 0.31	0.41 ± 0.07	15.1	-
1529	surface	BW	11.9	- 0.68	5.7 ± 0.27	0.25 ± 0.04	22.8	-
BW average (n=10)			7.9	-0.41	6 ± 0.4	0.26 ± 0.06	23.3	4 ± 1
Standard deviation			2.55	0.16	0.75	0.1	7.05	3
1507	bottom	SW	22.5	- 0.9	6.2 ± 0.24	0.19 ± 0.03	32.6	3 ± 1
1508	bottom	SW	22.4	- 0.87	7.2 ± 0.26	0.19 ± 0.02	37.8	1 ± 0.6
1530	bottom	SW	21.9	- 0.94	5.1 ± 0.37	0.14 ± 0.03	36.4	-
1507	7 m	SW	21.5	- 0.97	5.4 ± 0.22	0.16 ± 0.03	33.7	1 ± 0.6
SW average (n=4)			22.1	-0.92	5.9 ± 0.27	0.17 ± 0.02	35.1	2 ± 0.8
Standard deviation			0.46	0.04	0.94	0.02	2.39	0.01

*- measurements were not carried out

10
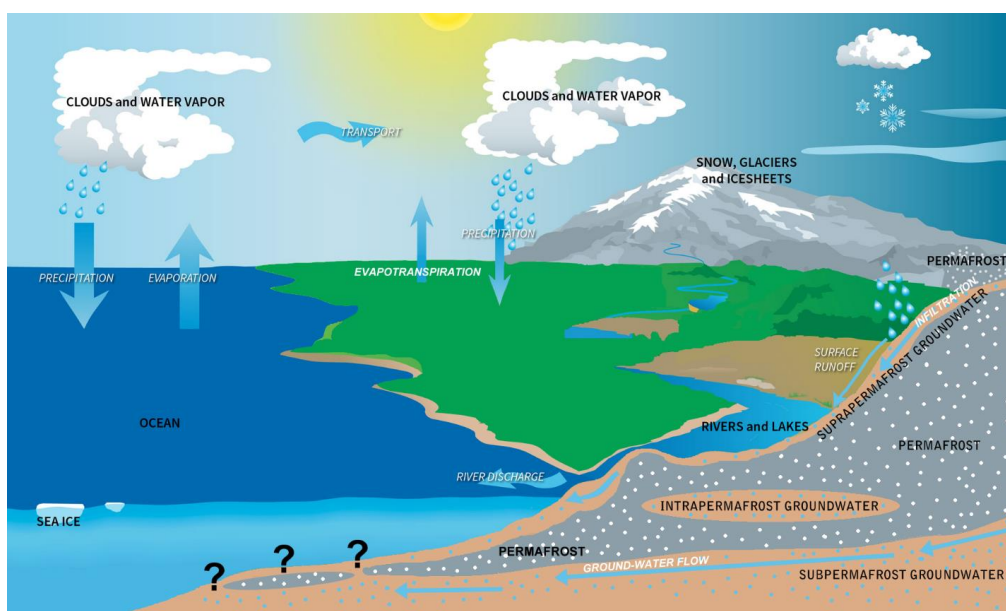
Figure 1: A view of the Arctic hydrological cycle showings key linkages among land, ocean, and atmosphere

5   **(modified from http://arcticchamp.sr.unh.edu/whatisarctichydro.shtml).**
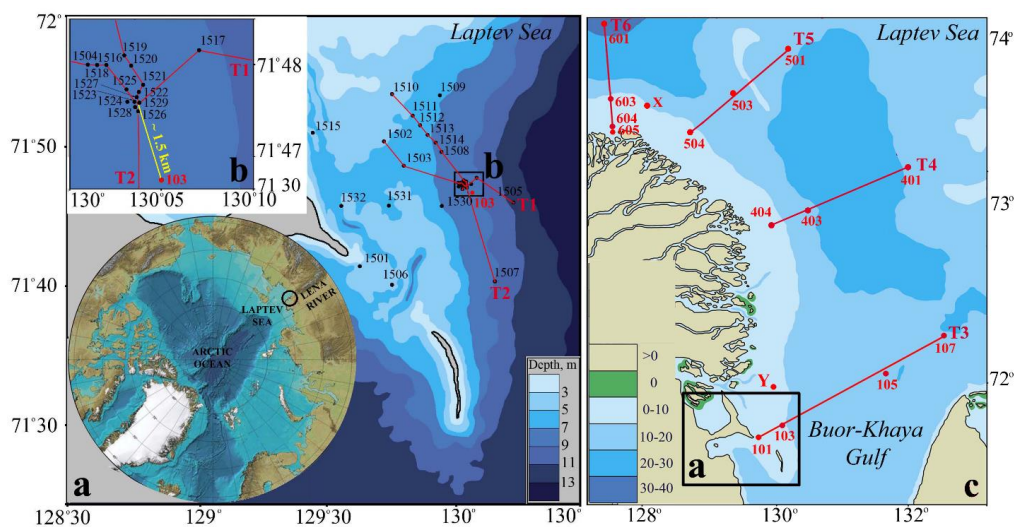
10

15

20

Figure 2: Study area: a) Study area in wintertime, b) Site of detail wintertime observations. Yellow line and number, the approximate distance between winter 1529 and summer 103 stations, c) Study area in summertime. Black dots – location and numbers of wintertime oceanographic stations, red dots - location and numbers of summertime oceanographic stations, red lines - oceanographic TS transects and their numbers.
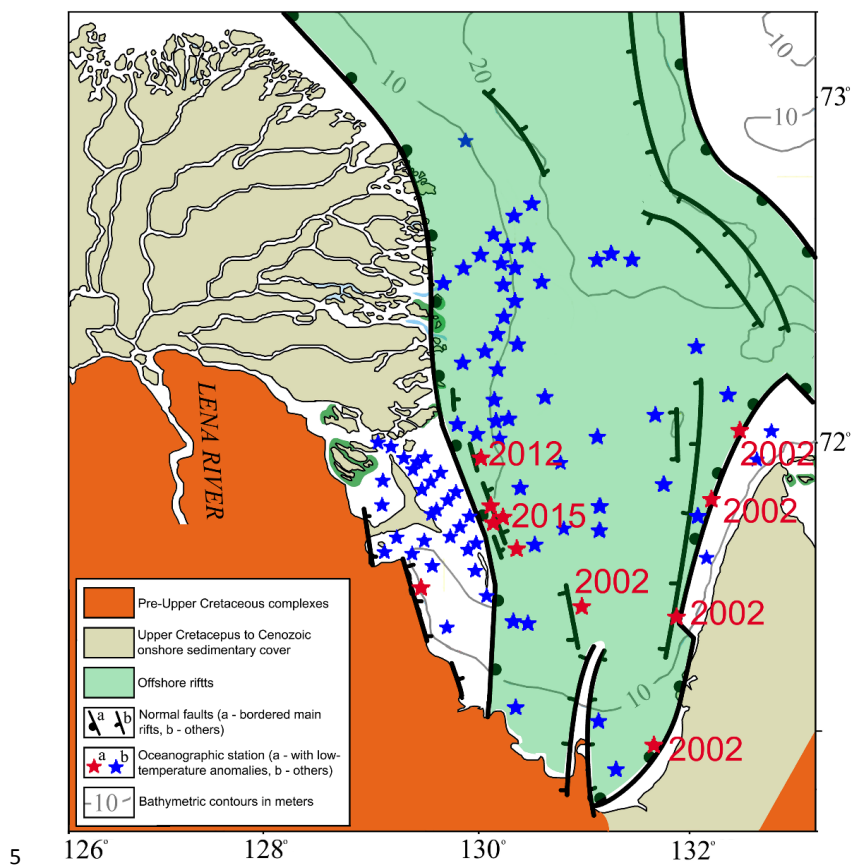
Figure 3: Ust Lena graben (after Drachev, et. al., 1998; Franke, et. al., 2001; Imaev, et. al., 2004). Numbers above the red stars indicate the years when the studies were carried out.
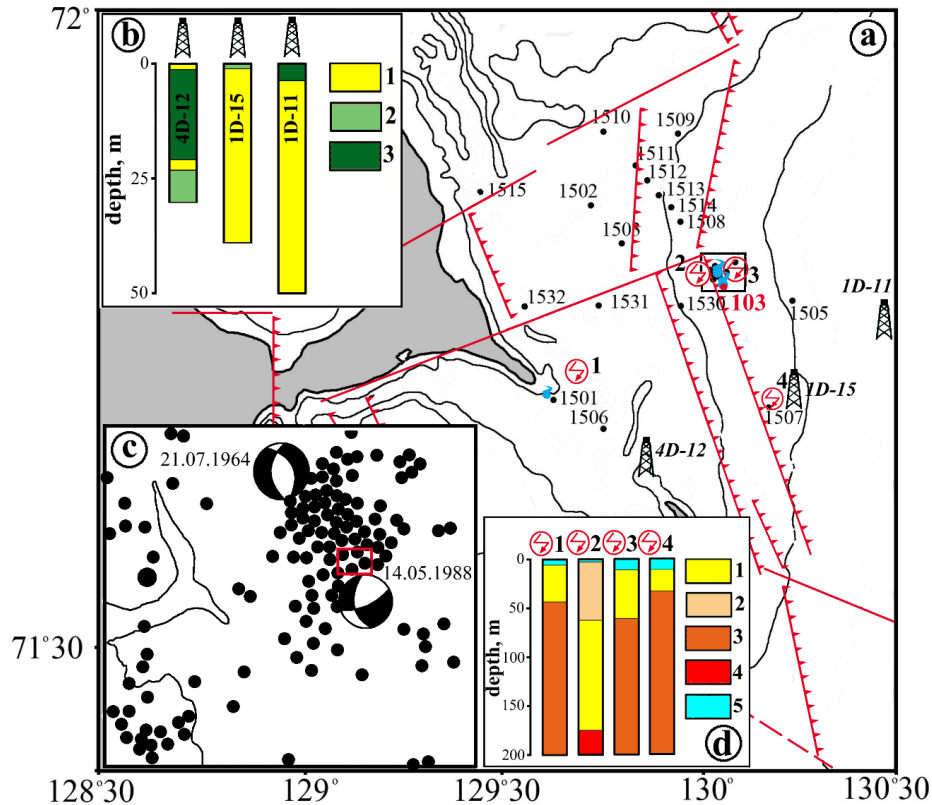
Figure 4: Location of drilling sites and oceanographic stations superimposed on a seismotectonic map modified from (Imaev et al., 2004).

    a) **The red lines with teeth are active faults; the red lines are active faults with kinematics, which have not yet been established; the red dotted lines are the presumed faults, the red rings are the geoelectric survey locations; the blue dots with a tail are the locations of SGD discovery.**

    b) **Grainsize composition of the drilling cores. 1) sands, 2) predominantly silts, 3) predominantly clay.**

    c) **The map of the earthquakes epicenters and focal mechanisms. The small dots are earthquakes with a magnitude of up to six. The large circles are earthquakes with a magnitude more than six, placed near the date of their occurrence.**

    d) **Resistivity in the bottom sediments (Ω m). 1) 0-5, 2) 5-10, 3) 35-100, 4) >350, 5) water. A table with more detailed information can be found in Supplementary Table 1.**
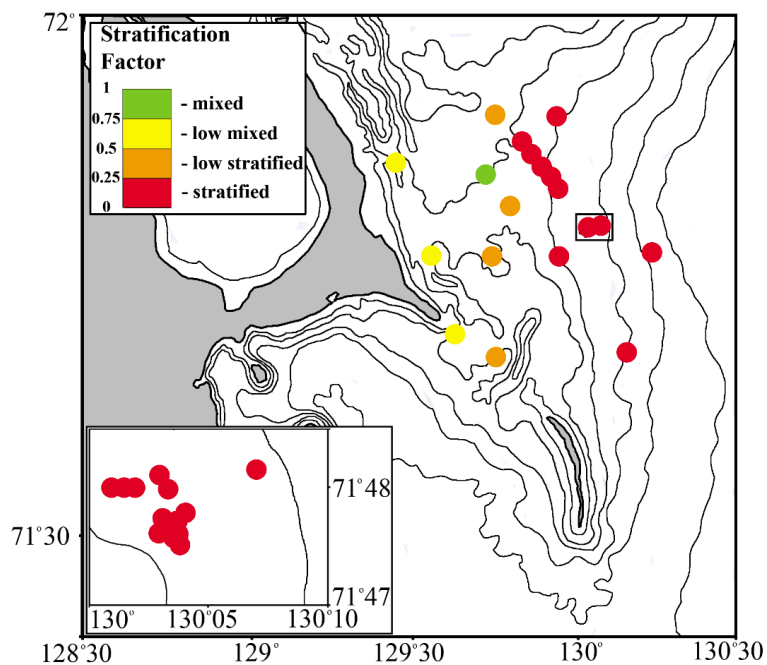
Figure 5: Wintertime stratification factor in the study areas.

5

The Cryosphere
Discussions

Open Access

EGU
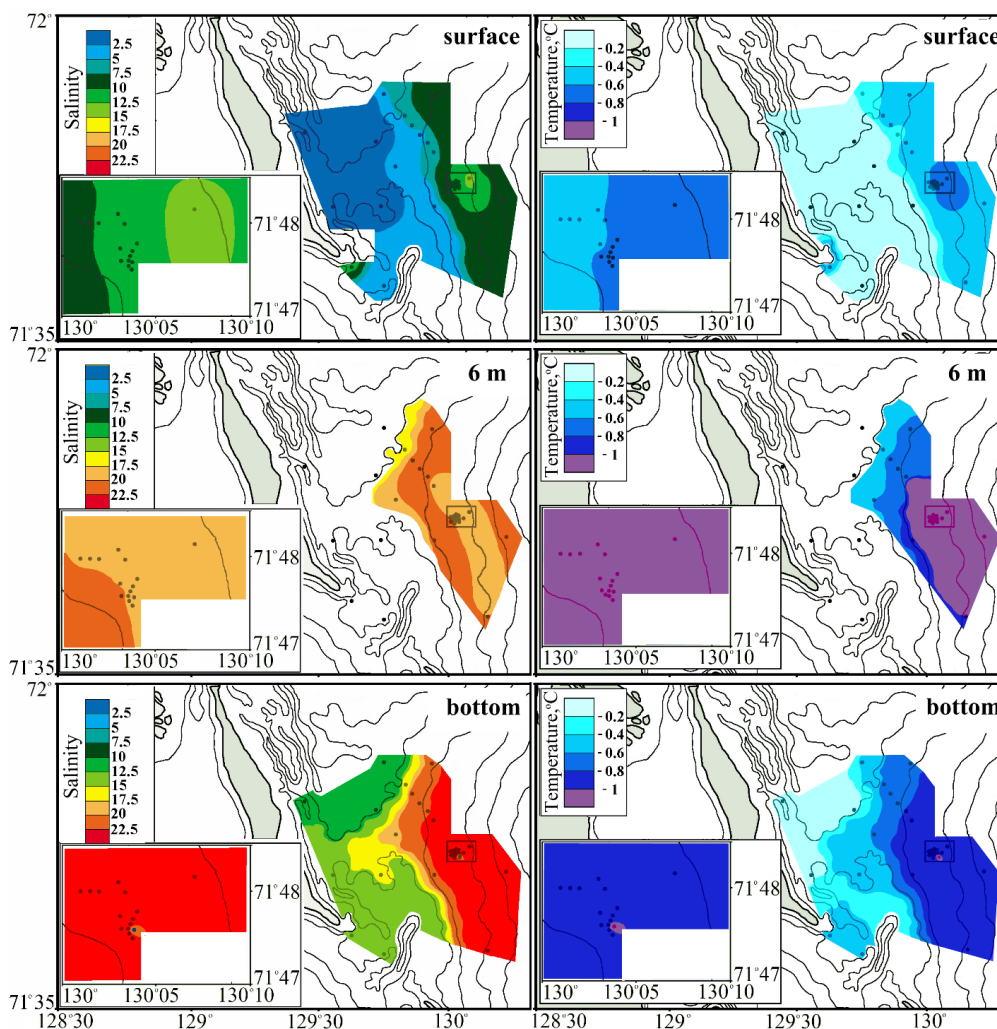
Figure 6: Salinity and temperature distribution of surface waters, 6 meters depth and bottom water horizons in the wintertime.

5

10

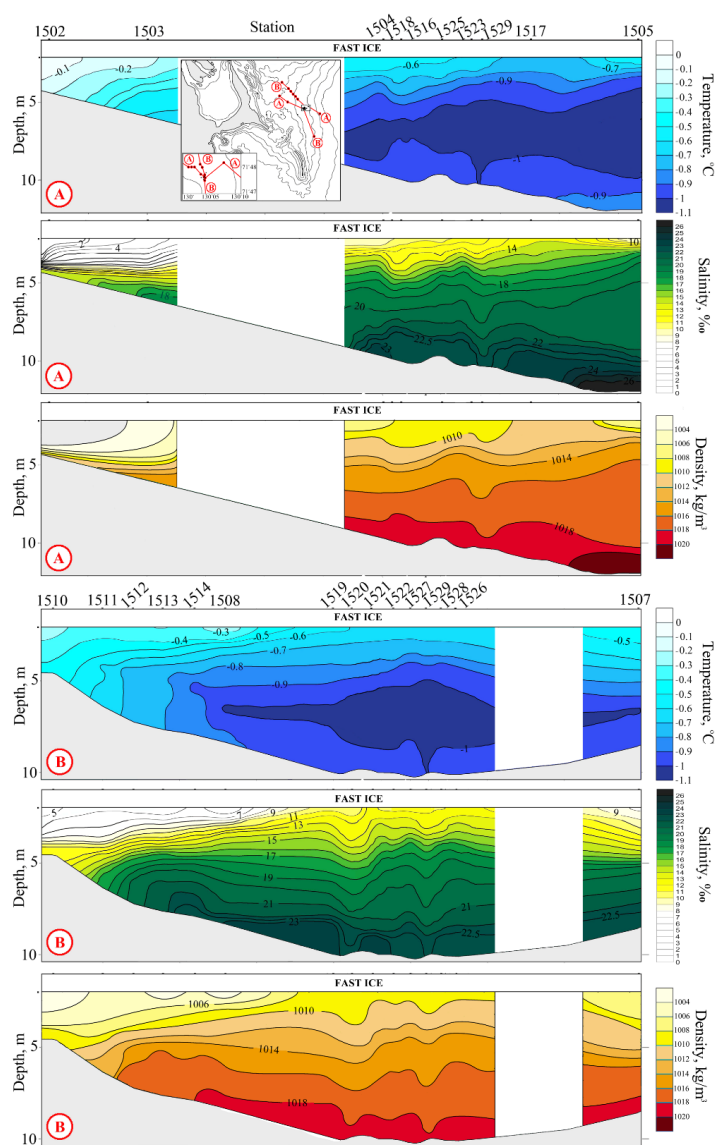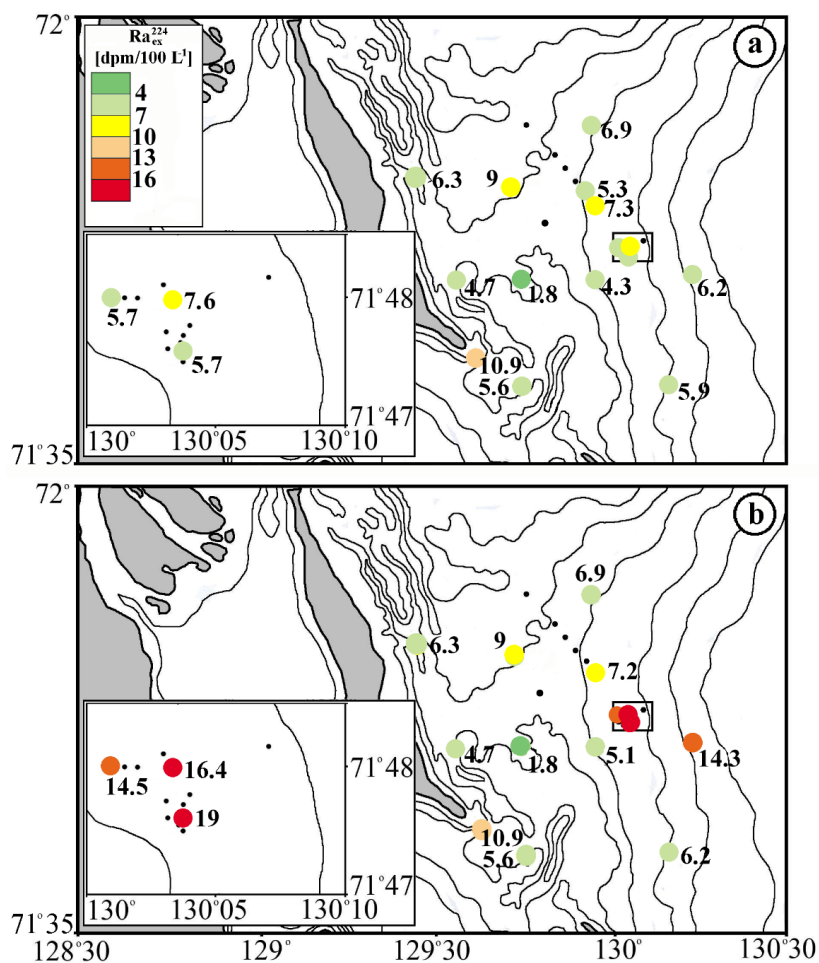**Figure 7: Vertical sections of salinity, temperature and density distribution in the wintertime.**

Figure 8: Wintertime distributions of ex²²⁴Ra in the surface (a) and bottom (b) horizons. In the shallow stations shown one values for the two horizons.

5

10
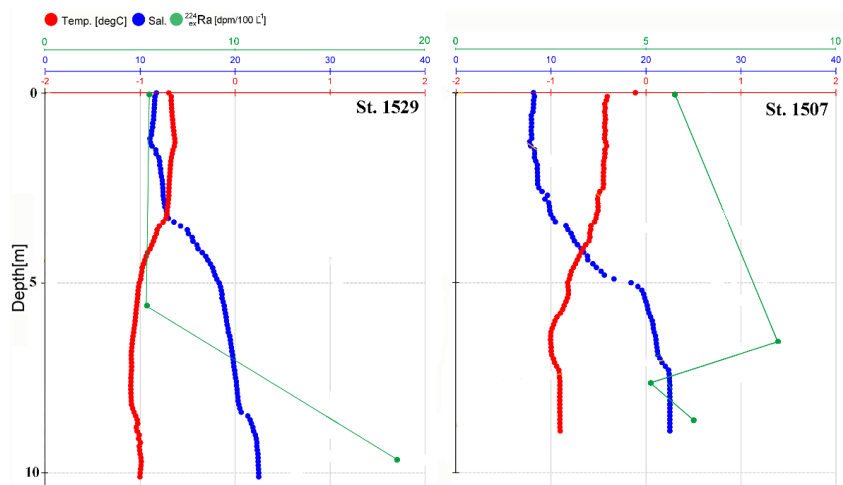
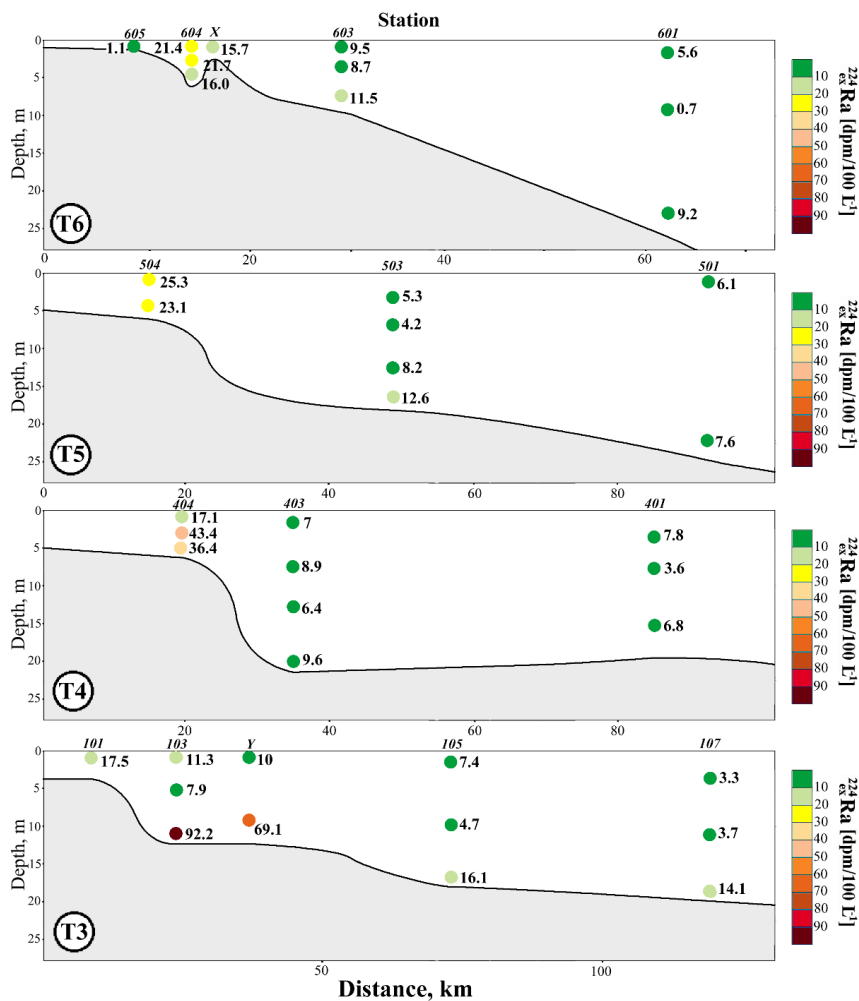**Figure 9: Wintertime vertical profiles of the water column.**

5

10

The Cryosphere
Discussions
Open Access
EGU

Figure 10: Summertime (September 2013) vertical distribution of ex^{224}Ra in the Lena Delta. Sta Y (72°N, 130°E) has been included in transect T3. A table with more detailed information can be found in Supplementary Table 2.
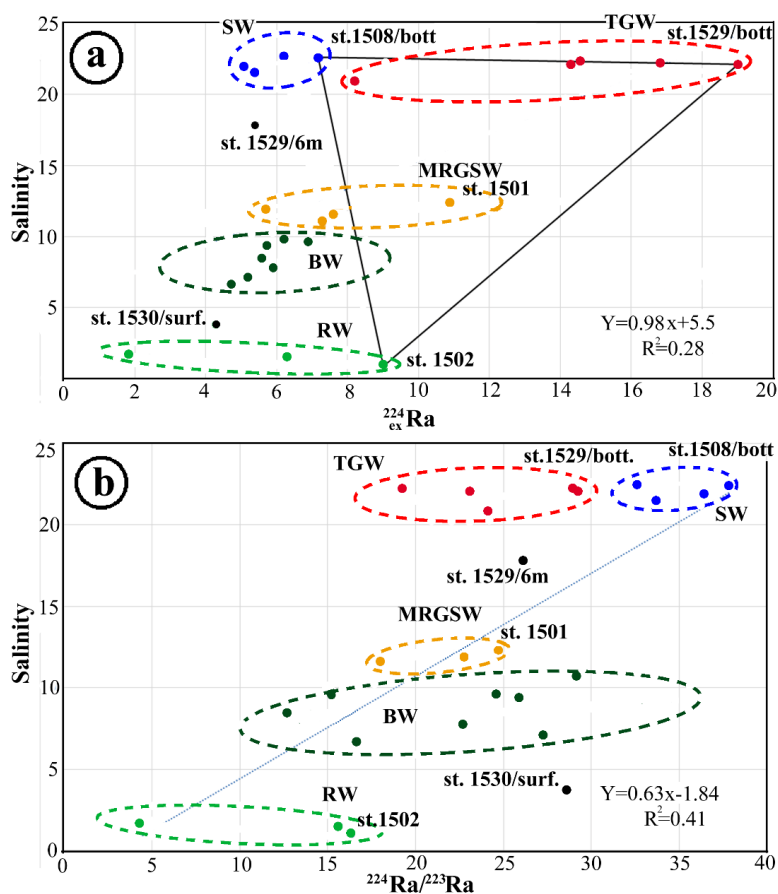
5

10

Figure 11: Salinity vs. ^{224}Ra (a) and ^{224}Ra/^{223}Ra (b) in the wintertime.

 a) **The three main water mass endmembers are identified in this diagram: River water (RW - light green dots), seawater (SW - blue dots), transformed ground water (TGW - red dots); and two derivatives from main water mass because of mixing: mixing river and seawater (BW - dark green dots), mixing river, ground and sea water (MRGSW - yellow dots).**

 b) **Similar as the mixing diagram panel (a) but using the ^{224}Ra/^{223}Ra ratio. The straight line represents the theoretical mixing line derived from the major radium sources.**
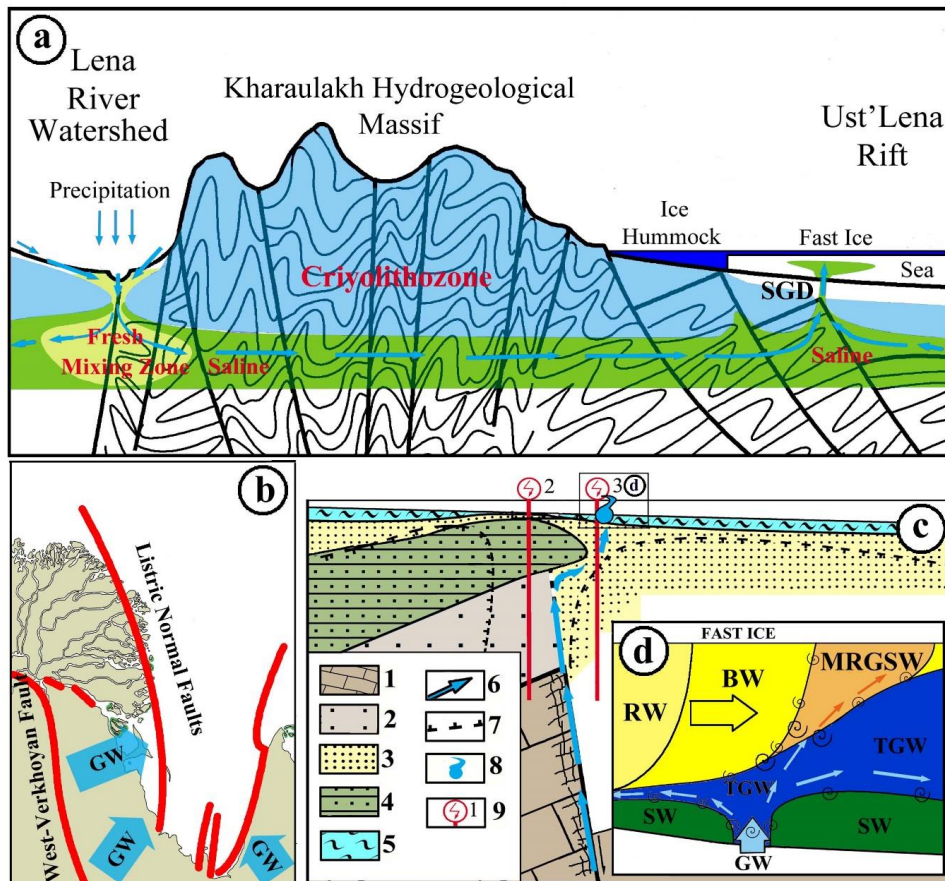
Figure 12: The mechanistic scheme of recharge, transport and discharge of submarine pressured groundwater.

a) The general vertical scheme of recharge, transport and discharge of submarine pressured groundwater.

b) The spatial scheme of groundwater transport in the Kharaulakh Hydrogeological massif.

c) The vertical scheme of groundwater transport and submarine discharge in place of tectonogenic talik based on TEM and drilling data. 1) metamorphic bedrock of Pre-Upper Cretaceous complexes, 2) substratum, 3) sands, 4) aeolian Quaternary material, 5) recent bottom sediments, 6) direction of movement of groundwater, 7) border of permafrost, 8) SGD, 9) place and number of TEM.

d) The scheme of water masses mixing near the location of SGD.
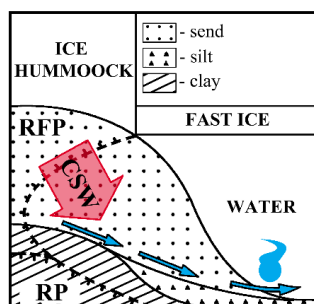
15

Figure 13: Scheme of cryogenic squeezing out of brine (CSB) and water-soluble salts from ice formation zone into warmer unfrozen parts of the sediments. RFS – recently frozen soil. RP- relict permafrost.

5

10

15

20